Spontaneous Structuration of Biohydrogels by Membrane-Free Osmosis

Emilie Guilbert, Clément de Loubens, Alice Vilotte, Christophe Schmitt, Deniz Gunes, Hugues Bodiguel

ADVANCED FUNCTIONAL MATERIALS
www.afm-journal.de

Spontaneous Structuration of Biohydrogels by Membrane-Free Osmosis

Emilie Guilbert, Clément de Loubens, Alice Vilotte, Christophe Schmitt, Deniz Gunes, and Hugues Bodiguel**

Many bio-hydrogels are prepared thanks to the addition of divalent ions. These gels usually exhibit partial ionic selectivity, a feature is leveraged to instigate an osmotic flow during the gelation process across a range of bio-hydrogels. A simple experimental setup consisting a glass capillary filled by the reactant solution is taken as an advantage, brought into contact with a reservoir of calcium chloride. Direct observation allows to characterize the gelation kinetics, the permeability and the selectivity of several gels, including some made of protein aggregates, pectin, and alginate. It is shown that these intrinsic properties, coupled with appropriate gelation kinetics, intricately govern the osmotic flow induced by the chemical potential difference of the calcium chloride ions imposed during gel formation, consistent with the Kedem–Kashalsky equation. The forming gel acts as a semi-permeable membrane for calcium chloride ions. The consequences of this osmotic flow are of potentially great interest since it triggers an increase of the gel concentration close to its boundary, opening the road to their spontaneous structuration. The formation of this dense shell is well accounted for the combination of a mass balance and a kinetic model.

1. Introduction

Biohydrogels are an assembly of low-volume fraction bio-based polymers or colloidal particles, which are widely used in material science. In biological tissues, biohydrogels serve as scaffolds for cells and have the particularity of presenting chemical and physical gradients, which are essential for organ development. [1,2]

Consequently, transport mechanisms relevant to the micro- and mesoscale structuring of hydrogels are highly relevant for tissue regeneration technologies,[3,4] e.g., to produce perfusable vessels or multilayered solid filaments. Moreover, the interest in gradient hydrogels is broader than regenerative medicine.[5,6] Among others, microencapsulation technologies rely on the possibility to control the microstructure of biohydrogels with applications as diverse as flexible electronics[7] or food science.[8,9] Gradient polyelectrolyte hydrogel (i.e., a gel exhibiting a spatial concentration gradient and as a result a gradient of related properties) membranes were as well developed to overcome technological limitations of asymmetric ionic membranes for osmotic energy generation.[10] The main limitation for the development of these new materials is the associated technical complexity of the structuring processes which are generally based on several sequential steps.[6]

In biological organisms, one specific role of the hydrogel is to control the exchange of molecules between different compartments.[11] This is achieved thanks to their partial-selectivity. In this respect, hydrogel membranes[12] are used for water desalination[13] or energy conversion.[14] For example, electric-eel-inspired power sources were designed by using a repeating sequence of cation- and anion-selective hydrogel membranes.[15] Partial selectivity can be seen as an energy barrier that must be overcome for solute molecules to diffuse into or through the material.[16] This energy barrier is due to charge interactions at nanometric scales between the solute and the material.[17] Consequently, efficient selectivity can be achieved for hydrogel if its structure can be controlled at the nano-scale to overcome its low pore density.[14,18]

In this paper, we show that even for low macromolecular concentration hydrogels, where significant selectivity is not anticipated, an osmotic flow can occur as a result of partial selectivity in ions. This flow induces the spontaneous formation of gradient biohydrogels. In the framework of semi-permeable membranes,[16,19] membrane selectivity to solute molecules is characterized by the reflection coefficient σ; we have $\sigma \to 1$

E. Guilbert, C. de Loubens, A. Vilotte, H. Bodiguel
Univ. Grenoble Alpes, CNRS
Grenoble-INP
Lab. LRP UMR 5520, F-38000 Grenoble, France
E-mail: clement.de-loubens@univ-grenoble-alpes.fr; hugues.bodiguel@univ-grenoble-alpes.fr
C. Schmitt, D. Gunes[+]
Nestlé Research
Nestlé Institute of Food Sciences
Vers-Chez-Les-Blanc, Lausanne CH-1000, Switzerland

The ORCID identification number(s) for the author(s) of this article can be found under https://doi.org/10.1002/adfm.202400888

[+]Present address: Department of Chemical Engineering and Center for Food and Microbial Technology, KU Leuven, Leuven 3001, Belgium

DOI: 10.1002/adfm.202400888

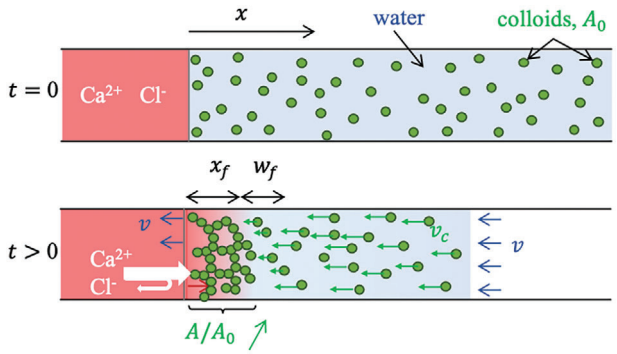

Figure 1. Schematic diagram of spontaneous structuring due to an osmotic flow, during gelation of colloidal suspensions. **Top**: A solution of calcium chloride (in pink) is put into contact with a colloidal suspension (in green) at an initial concentration A_0 in a glass capillary. **Bottom**: Calcium chloride ions diffuse inside the suspension (pink gradient) and induce their gelation over a distance x_f, which increases with time. The gel being partially selective to calcium chloride (white arrows), the osmotic pressure difference between the suspension and the $CaCl_2$ solution induces an osmotic flux v. This osmotic flux advects the non-gelled colloids with a velocity $v_c = v$. v_c decreases in the transition zone between the gel and liquid phases w_f up to the complete gelation of the colloids ($v_c = 0$ when $x < x_f$), whereas the water permeates through the gel. Consequently, the concentration in colloids increases in the region of transition between the gel and the liquid, leading to a concentration gradient in colloids.

for fully selective membranes and $\sigma \to 0$ for non selective ones. In the dilute regime for the solute, the Kedem–Katchalsky equation[20,21] links the osmotic flux v (per unit area) to the total pressure difference across the membrane ($\Delta P - \sigma\Delta\Pi$), where $\Delta\Pi$ and ΔP are the osmotic and mechanical contributions, respectively. The Kedem–Katchalsky equation reads

$$v = \frac{\kappa}{\eta L}(\Delta P - \sigma\Delta\Pi) \tag{1}$$

where η is the solvent viscosity viscosity, L the thickness of the membrane, and κ its permeability.

Our aim is to show that the partial selectivity of biohydrogels to ions causes an osmotic flux of their solvent during their gelation. By transporting the biomacromolecules while they are not yet gelled, this flux spontaneously creates gradients hydrogel. These phenomena are quantified in a shallow cell with a 1D flow in which a suspension of protein aggregates is put into contact with a droplet of calcium chloride, **Figure 1**-top. The kinetics of gelation of the aggregates during the diffusion of calcium chloride is observed using brightfield microscopy. These experiments reveal the emergence of a flux of solvent through the gel in formation, which depends on the calcium chloride concentration, Figure 1-bottom. By controlling the pressure difference between the suspension of protein aggregates and the droplet of calcium chloride, we show that this phenomenan is due to the partial selectivity of the hydrogel to calcium chloride. We extend this analysis to two others systems, namely pectin and alginate. In addition, these experiments allow a direct determination of the reflection coefficient σ and the permeability κ of the gel. Finally, we experimentally investigate and model a striking consequence of this osmotic flux: the spontaneous formation of a concentration gradient, Figure 1-bottom.

2. Results

2.1. Osmotic Flow During Gelation

The kinetics of gelation of a suspension of whey protein aggregates is studied by creating a flat front between a solution of $CaCl_2$ and the suspension in a thin rectangular glass capillary, **Figure 2**A. The physico-chemical conditions of preparation of the aggregates lead to a suspension composed of sub-micrometric and non-gelled aggregates of 70 nm radius. It is well established that the addition of $CaCl_2$ to such a suspension induces a sol–gel transition.[22,23] Gelation results from both screening of electrostatic interactions and specific binding of calcium ions to the aggregates.[23] A drop of $CaCl_2$ solution is gently put into contact with a thin glass capillary which contains the suspension of aggregates. The gelation is followed by bright-field microscopy which is possible due to a small decrease in the transmitted light intensity due to the gelation of protein aggregates (see details in Supporting Information). Figure 2B shows a spatio-temporal map of the light intensity, which allows us to define the position of the gelation front x_f in the zone where the gradient of light intensity is maximal (red dashed line). Several experiments are performed by varying the $CaCl_2$ concentration in the drop C_0 while the protein concentration A_0 is kept constant. The insert in Figure 2C shows that the front position x_f appears with a time delay that decreases from 1 to 10 s when C_0 is increased from 0.37 to 5.57 M. Then, x_f increases sharply, which is a signature of a reaction-limited kinetics. At long time scales, x_f increases more slowly and asymptotically follows a growth as $t^{1/2}$, which is characteristic of diffusion-limited kinetics.

These gelation kinetics are crudely simple with a simplified reaction-diffusion model (see Supporting Information for details). We consider that calcium ions diffuse in the suspension of protein aggregates with a diffusion coefficient D_0 and cross-link the protein aggregates. Each protein aggregate has n reaction sites for calcium ions (n being typically between 5 and 10[23]). Despite the complexity of cold-set gelation of protein aggregate by ionic interactions,[23] we make the first-order approximation that the calcium consumption rate is given by $nkAC$, k being the kinetic constant of the reaction. The kinetics of gelation is described by the following a dimensionless set of reaction-diffusion equations (see details in Supporting Information)

$$\partial_{\tilde{t}} c - \partial^2_{\tilde{x}} c = -\frac{n}{r} ac \tag{2}$$

$$\partial_{\tilde{t}} a - \epsilon \partial^2_{\tilde{x}} a = -ac \tag{3}$$

where $c = C/C_0$ and $a = A/A_0$ are the reduced concentrations of $CaCl_2$ and proteins, respectively, which are normalized by their boundary values ($C = C_0$ for $x < 0$ and $A = A_0$ for $x \to \infty$), $\tilde{x} = x/\sqrt{D_0/kC_0}$ and $\tilde{t} = tkC_0$ are the non-dimensional space and time variable. $r = C_0/A_0$ and $\epsilon = D_a/D_0$ are the concentration and diffusion coefficient ratios.

Since the experiments are carried out in the limit where ϵ and n/r are much smaller than unity, the dimensionless position of the front of gelation $\tilde{x}_f(\tilde{t})$ is given by a single mastercurve which is determined numerically as detailed in the Supporting Information (dashed line in Figure 2C). We observe that the experimental data (symbols in Figure 2C) overlap very well on this mastercurve,

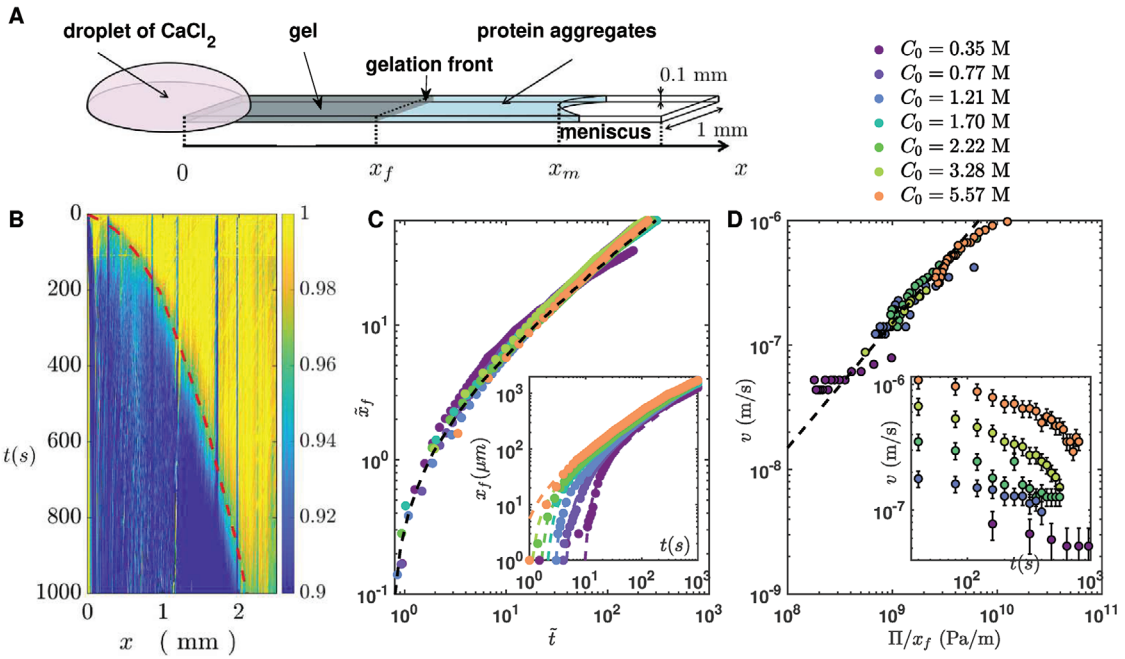

Figure 2. A) Sketch of the experimental set-up. A droplet of calcium chloride solution is put into contact at time $t = 0$ with a glass capillary that contains a suspension of protein aggregates. The gelation front position x_f is tracked by monitoring the changes in light intensity. The flux of the solvent trough the gel is measured thanks to the position of the meniscus x_m. B) Spatio-temporal image of the normalized grey-scale intensity along the length x of the capillary; the dotted red line represents the gelation front position x_f for a $CaCl_2$ concentration of $C_0 = 5.57$ M. C) Non-dimensional front position $\tilde{x}_f = x_f/\sqrt{D_0/kC_0}$ versus non-dimensional time $\tilde{t} = tkC_0$ for various C_0. Dots: experimental data. Dotted lines: solution of the reaction-diffusion model (Equations 2 and 3). Inset: same data in physical units. D) Osmotic flux v versus the ratio of the osmotic pressure of the calcium chloride solution Π by the length of the formed gel at a given time, $x_f(t)$. v is determined from the velocity of the rear meniscus. The dashed line is the best linear fit to the data (slope 1.5×10^{-16} m$^2 \cdot$ s$^{-1} \cdot$ Pa^{-1}). Insert: Same data, plotted as a function of time.

for $k = 2 \times 10^{-1}$ L mol^{-1} s^{-1} and $D_0 = 1 \times 10^{-9}$ m^2 s^{-1}. Note that the calcium chloride concentration is varied by more than an order of magnitude. The value of D_0 is very close to the diffusion coefficient of Ca^{2+} in water at 25°C (=1.16×10^{-9} m^2 s^{-1}[24]). We tentatively conclude that the gelation of protein aggregate is solely governed by a reaction-diffusion mechanism characterized by a reaction-limited regime followed by a diffusion-limited one.

Despite its apparent simplicity, the gelation of protein aggregates induces a flow inside the capillary, which is directed toward the calcium chloride reservoir. Indeed, the meniscus between the suspension of aggregates and the air inside the capillary (Figure 2A) move in the direction of the calcium chloride reservoir during the gelation. The water flux v is derived by following the position of the rear meniscus for calcium chloride concentration ranging from 0.35 to 5.57 M. The insert of Figure 2D shows that v decreases with time and increases when C_0 is increased; from 1 µm s^{-1} for $C_0 = 5.57$ M to 0.1 µm s^{-1} for $C_0 = 0.35$ M, at the beginning of gelation. These data are directly accounted for by the Kedem–Katchalsky equation (Equation 1 with $\Delta P = 0$), where the length L over which water permeates corresponds to the length of the gel, $x_f(t)$, and where $\Delta\Pi$ is the osmotic pressure Π of $CaCl_2$ in the droplet (calculated from,[25] see Supporting Information Figure S2). Indeed, as shown in Figure 2D, data from different C_0 collapse on a linear relationship with respect to Π/x_f. From the slope we find that the product of the permeability and the reflection coefficient $\kappa\sigma$ equals 1.4×10^{-19} m^2. This implies that this product is constant in time and independent of the calcium concentration. The flatter trend observed at the lowest tested concentration may stem from some evolution of these parameters over time, but the data in question suffer from greater uncertainty compared to other data, limiting their ability to fully support such an interpretation.

This first set of experimental investigations of the gelation of protein aggregates through the diffusion-reaction of calcium chloride highlights the emergence of an osmotic flow during the gelation that we attribute to the partial selectivity of the gel to calcium chloride. This partial selectivity has for a consequence a flux of water through the gel in formation whose magnitude is proportional to the osmotic pressure of the calcium chloride. To go further, we impose a pressure difference ΔP in the capillary to determine simultaneously the values of the gel permeability κ and the reflection coefficient σ.

2.2. Permeability and Reflection Coefficient of Hydrogels

In order to determine independently the permeability κ and the reflection coefficient σ, the capillary is connected to a reservoir which allows us to impose a mechanical pressure difference ΔP between the two sides of the gel. One side of the capillary is in contact with the droplet of $CaCl_2$ solution, whereas the other side is connected to the reservoir, which is filled by the suspension of aggregates doped with fluorescent particles (5 µm diameter). The two solutions are brought into contact without applying any

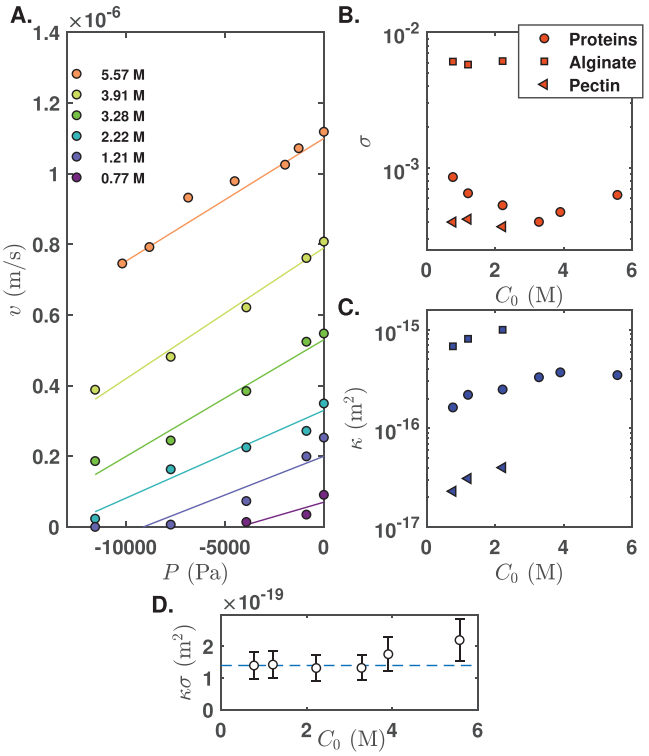

Figure 3. A) Flux v as a function of the relative pressure P in the suspension ($P = -\Delta P$), for the gels of protein aggregates at different C_0 (see legend). The lines are the best linear fits to the data. B) Reflection coefficient of gels of alginate, pectin and protein aggregates for different C_0 values. C) Permeability of gels of alginate, pectin and protein aggregates for different C_0 values. D) Product $\kappa\sigma$ for protein gels, the dotted line corresponds to the value found during the gelation (see Figure 2D), $\kappa\sigma = 1.4 \times 10^{-19}$ m^2.

pressure. We wait until the gel is 1 cm long. Then, we measure the flux v for various negative applied pressures. v is determined by averaging the velocities of tracer particles located far from the gel front. As shown in **Figure** 3A, an affine relation is found, in agreement with the Kedem–Katchalsky equation (Equation 1). For the lowest calcium chloride concentration studied, it was even possible to cancel out the total flux, meaning that the mechanical pressure balances the effective osmotic one $\sigma\Pi$. σ and κ are determined by fitting the experimental data with (1). The values of the two coefficients are approximately independent of C_0, circles in Figure 3B,C. This observation is probably due to the fact, that, in the condition studied where the calcium is in large excess as compared to the proteins, the cross-linking density of the gel is in a first approximation independent of the calcium concentration. The mean value of the permeability $\kappa = 2.8 \times 10^{-16}$ m^2, which is consistent with previously reported values.[26] The reflection coefficient is very low, $\sigma = 5.3 \times 10^{-4}$, which means that gel is poorly selective. The product $\kappa\sigma$ remains constant with C_0, Figure 3D. $\kappa\sigma$ is $\approx 1.5 \times 10^{-19}$ m^2, which is in full agreement with the value found during the gelation (see previous section).

The same experiments are carried out with solutions of pectin and alginate which can be cross-linked by calcium ions,[27–29] similarly to the protein aggregate suspensions. For these systems, the fluorescent particles also move towards the solution of $CaCl_2$ when ΔP is zero. We also observe linear trends between v and ΔP which allows us to measure κ and σ for these hydrogels. Similarly to the gels of protein aggregates, these coefficients are almost independent on C_0, Figure 3B,C. The reflection coefficients are also small compared to unity: $\sigma = 7 \times 10^{-3}$ and $\sigma = 4 \times 10^{-4}$ for alginate and pectin gels, respectively. The permeabilities are $\approx 8 \times 10^{-16}$ and 3×10^{-17} m^2. For alginate gels, the value is of the same order of magnitude that previously reported ones (e.g., $\kappa \simeq 2 \times 10^{-15}$ m^2 in ref. [30]).

To sum up, by combining a mechanical and osmotic pressure difference, we made it possible to determine independently both permeabilities and reflection coefficients of different hydrogels. The selectivity of hydrogels to ions appear to be a generic phenomenon, while the value of σ could be very small.

2.3. Spontaneous Formation of Gradient Hydrogels

The osmotic fluxes evidenced and characterized above during gelation are advecting the coloids before they gelate, i.e., for $x > x_f$. One can therefore expect an increase in their concentration in the gel phase. Due to their lower diffusion coefficient, this effect is simpler for protein aggregates than for the other systems tested since, given the order of magnitude of the osmotic flux, concentration gradients could be established over length scales greater than $D_a/v \approx 10$˜µm. In order to characterize this phenomenon, protein aggregates are covalently labeled with a fluorescent probe (see Experimental Section for details). Gelation experiments are carried out in an open glass capillary (Figure 2A) and the profile of protein concentration is measured by fluorescent microscopy imaging, the fluorescence intensity being proportional to the total protein concentration.

Figure 4A,B shows two examples of the temporal evolution of the normalized total protein aggregates concentration w along the length of the capillary, for calcium chloride concentrations of 1.7 and 5.57 M. As time elapses, w progressively increases, especially in the vicinity of the inlet. The profiles then stabilize as the gelation phenomenon finishes. Two zones can be distinguished. The first is located near the interface with the $CaCl_2$ solution ($\tilde{x} \lesssim 5$, corresponding in the physical unit to $x < 150 -$ 350µm, depending on the calcium chloride concentration). At the end of the gelation period, the concentration in aggregates in this region, namely the sell, is highly localized and increasing by 3.5 and 1.5-fold for $C_0 = 5.57$ and 0.77 M, respectively. In the second zone, the concentration profile is almost flat and the increase in concentration is much more moderate than in the shell. At low C_0, the aggregate concentration in the gel is almost equal to the concentration in the solution A_0 ($w \simeq 1$). However, the concentration is multiplied by 1.5 for the largest C_0 values investigated.

We propose a simple deterministic model based on the following physical aspects and contributions: i) the aggregates are advected homogeneously by the osmotic flow far from the front of the gel, ii) they are trapped by the gel in the width of the gelation front and do not move as soon as the gel is formed, iii) the osmotic flow is described by the Kedem and Katchasky equations (Equation 1), iv) the gelation front position x_f is modeled by reaction-diffusion equations, which are not coupled to the osmotic flow (Equations 2 and 3). Introducing these contributions and conditions in a mass balance equation (see details in

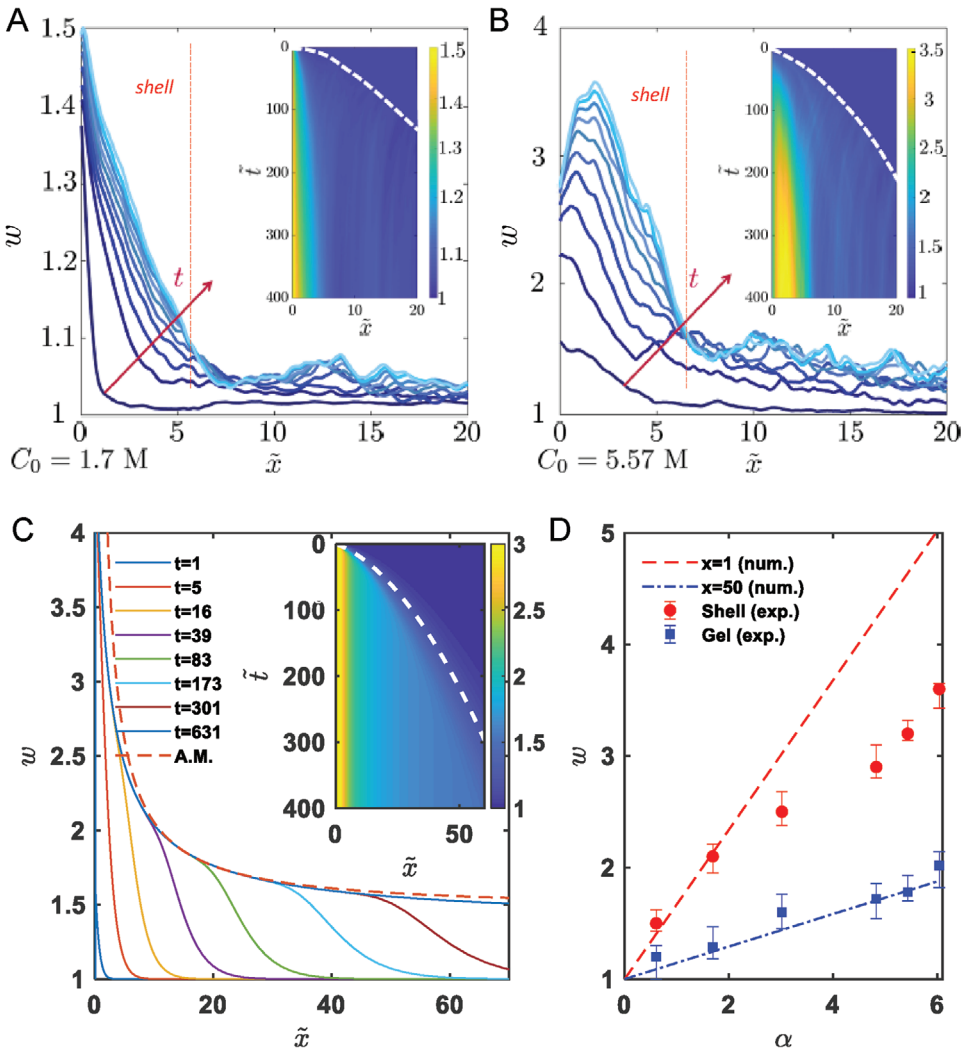

Figure 4. A,–C) Normalized protein concentration w profiles for different times. In inset, the full spatio-temporal image of w is shown. The white dashed line represent the front position $\tilde{x}_f(t)$, which was determined independently. Subfigures A and B are experimental results (for $C_0 = 1.7M$ and $C_0 = 5.57M$, corresponding to $\alpha = 1.7$ and 6.0), subfigure C displays the numerical results obtained for $\alpha = 4$, see Supporting Information for details. The dashed line is the asymptotical analytical solution, $w = 1 + \tilde{x}_f \dot{\tilde{x}}_f$. D) Normalized protein concentration w estimated in the shell close to $\tilde{x} = 0$ (circles) and in the uniform gelled region (squares) as function of α. Dashed and dash-dotted lines correspond to the numerical results at $\tilde{x} = 1$ and $\tilde{x} = 50$.

Supporting Information) leads to the following governing equation for the total protein concentration w:

$$\partial_{\tilde{t}} w + \frac{\alpha}{\tilde{x}_f(\tilde{t})} \partial_{\tilde{x}}(aw) = 0 \tag{4}$$

where a is the reduced concentration of free aggregates introduced in the protein flux to account for the mobility of the aggregates, and where

$$\alpha = \frac{\kappa \sigma \Pi}{\eta D_0} \tag{5}$$

The resolution of the above equation leads to establishing evidence for the development of concentration gradients which are very similar to the experimental ones: a dense shell is formed close to $\tilde{x} = 0$, adjacent to a uniform region where the aggregate concentration is slightly greater than the initial one. The model introduces a single non-dimensional parameter α which compares the osmotic flux to the gelation kinetics. According to the model, the relative concentration increment $(w - 1)$ in the gel phase is proportional to α (more details are given in Supporting Information). This is in agreement with the experimental results obtained for various osmotic pressure values, as shown in Figure 4, both in the core at long distance and in the denser shell. Moreover and despite the simplicity of the approach, the model accounts semi-quantitatively for the experimental data, taking values of the concentration increment at $\tilde{x} = 1$ and $\tilde{x} = 50$.

Some differences remain to be understood, e.g., the progressive increase of the protein concentration in the shell and the overestimation of the shell concentration for the largest values of α (see Figure 4). In fact, when the osmotic flux is large ($\alpha \gg 1$), the model is no longer valid since one would need to add this convective flux to the reaction-diffusion set of equations,

making the problem fully coupled. The model also introduces an ill-defined question at short times (and also distances), in the reaction-limited regime, since the gel is not formed yet and thus cannot trigger an osmotic flow. The description finally suffers from the hypothesis that α remains constant in time. In particular, the product $\kappa\sigma$, though independent of the calcium chloride concentration, probably depends on the protein concentration. Addressing these limitations would demand a significant improvement of the theoretical description, which falls out of the scope of the present paper which aims to provide a first order description of the phenomenon and experimental data on the basis of a simplified physical model.

With a few simplifications detailed in the Supporting Information, the model also has a long-time asymptotic analytical solution, simply given by $w = 1 + \alpha/\tilde{x}_f\dot{\tilde{x}}_f$, where $\dot{\tilde{x}}_f$ is the non-dimensional time derivative of the front position. This result, shown in the dashed line in Figure 4, requires about the physical causes. The inverse proportionality with respect to the front position simply comes from the slowing down of the osmotic fluxes due to water permeation through the gel. The aggregates only accumulate in the vicinity of the reaction front, since they are simply advected at a larger distance and do not penetrate the gel phase. Thus, apparent front position velocity $\dot{\tilde{x}}_f$ also limits the concentration increase, since the aggregates do not have the time to accumulate when it is large. Interestingly, the existence of a uniform region ($w = cst$) comes from the fact that both effect compensate each other: $\tilde{x}_f\dot{\tilde{x}}_f = cst$ in the diffusion-limited regime where the front position increases asymptotically as the square root of time. On the contrary, we could interpret the existence of a shell as the consequence of the reaction-limited regime at short times, since the front position increases more rapidly than its velocity decreases in between the two asymptotic regimes.

The theoretical framework proposed has important practical consequences as it allows to predict the formation of a shell, i.e., the establishment of a concentration gradient near the interface of a gelified material. It provides a comprehensive description that could be used to enhance or limit this spontaneous structuration. Two main features are relevant. The first one is the non-dimensional parameter $\alpha = \kappa\sigma\Pi/\eta D_0$, which compares the order of magnitude of the osmotic flux with ionic diffusion. The concentration increase in the shell layer is indeed proportional to this parameter. It can thus be enhanced by increasing the osmotic pressure, the gel selectivity and permeability. The α parameter is inversely proportional to the product of the ionic diffusion coefficient with the solvent viscosity. Since both are related to each other ($D_0 \propto 1/\eta$), their product cannot be varied significantly. The second relevant feature is related to the gelation kinetics. As explained in the previous paragraph, the width of the shell, where the concentration gradient develops, is directly controlled by the gelation front dynamics. The gel concentration decreases until the transition between reaction-limited regime and the diffusive one. More precisely, the width of the shell was found to be a few units (typically 5) in the non-dimensional coordinates $\tilde{x}$. Coming back to physical quantities, the shell width is a few times the characteristic distance of the reaction-diffusion phenomenon, i.e., $\sqrt{D_0/kC_0}$. One thus needs to limit the reaction rate in order to obtain large shells, and vice versa.

3. Discussion and Concluding Remarks

It is evidenced in this work that different hydrogels act as semi-permeable membranes to ions. It is not surprising from a physical point of view because of the presence of charges on the gel constitutive elements. More striking is the observation that this selectivity - though small in the system studied - is effective during the gelation phenomenon itself, which is induced by calcium ions. As a direct consequence, an osmotic flow competes with the diffusion process and is quantitatively accounted for by the Kedem–Katchalsky equation. The simple experimental setup and protocol used in this study is of great interest for the characterization of hydrogels permeability and selectivity.

Let us emphasize the consequence of the simultaneity of the gelation and of the osmotic flow: it results in the spontaneous establishment of a concentration gradient in the gel. The concentration increase is predicted by using a simple mass balance equation, where colloids are advected by the osmotic flow in the non-gelled region, and kinetically arrested in the gelled one. Despite requiring refinements for more accurate predictions, the proposed model accounts for the gelation kinetics, the osmotic flux and the concentration increases. It highlights that the formation of a shell at the boundary of the gel is directly controlled by the gelation kinetics. More precisely, its width is controlled by the kinetics, and its concentration is by the osmotic flux. In this study, calcium chloride is used to induce both gelation and osmosis. It would be interesting to use another type of ions in order to be able to control both the width and concentration of the shell independently.

Concentration gradients in alginate-based hydrogels have been reported in many studies.[31–34] It has been proposed and modeled by several authors[31,33,35] that the dense layered formed near calcium (or other bounding ions) reservoir was due to a rapid binding of biomacromolecules by the ions, leading to a depletion zone. This depletion zone then drives the diffusion of free oligomers which increase the gel concentration. Coupled reaction-diffusion models indeed allow to account for concentration gradients. The mechanism proposed in this paper is very different since it is based on an osmotic flux driven by ion concentration difference between the two ends of the systems, without the need of a complex interplay between reaction rates and diffusion differences between species. While it is possible that the reaction-diffusion mechanism could be responsible for concentration gradients in alginate gels, it cannot apply to gels of protein aggregates due to their small diffusion coefficient. Furthermore, the quantitative consistency of the osmotic mechanism detailed in the present work strongly support this scenario for gels formed by low-diffusivity colloidal precursors. Regarding alginate gels, we report here that they exhibit a small but non negligible selectivity to calcium chloride ($\sigma = 7 \times 10^{-2}$), greater than measured for the gels of protein aggregates. It is therefore possible that in some cases, osmotic fluxes which have been neglected in previous work, could play an important role in addition to mechanisms based on reaction kinetics and on the difference in diffusion coefficients.

The gels used in this study exhibit a very low selectivity, and it was necessary to use very concentrated calcium chloride solutions to trigger an important concentration gradient. The

phenomenon described here can be directly transposed to more selective gels and lower ionic concentrations.

It offers promising perspectives in terms of biomaterials structuration, as the dense shell is formed spontaneously. For example, in a recent communication, using the same material, we reported about the fabrication core-shell fibers at high calcium chloride concentrations,[36] but not at low ones. It is clear that those previous observations directly correspond to the self-filtration phenomenon described here. Beyond material applications, the findings could also have implications in biological processes where hydrogels (e.g., mucosal barrier layers) are naturally building.

4. Experimental Section

Solutions: The solution of whey protein aggregates was prepared from WPI Prolacta 95, purchased from Lactalis Ingredients as a dry white powder with the following composition (in g/100g): protein 88.5 (65% β-lactoglobulin, 20% α-lactalbumin, 10% soluble caseins, 5% bovine serum albumin, and immunoglobulin), moisture 5.6, ash 1.9, fat 0.5, carbohydrates 0.14, Ca 0.35, K 0.35, P 0.21, Na 0.15, Mg 0.06, and Cl 0.01. A protein stock solution of 15% w/w was prepared by stirring the powder in deionized water at 4°C until complete dissolution, 0.02% of sodium azide (Sigma–Aldrich, CAS 26628-22-8) was added to prevent bacterial growth. The stock solution was then diluted to 8% w/w with 10 mM NaCl and the pH was adjusted at 7.0 pH with a 1 mol L^{-1} sodium hydroxide (NaOH) solution. Aggregates were obtained by heat treatment of the protein solution into 10 mL Pyrex tubes at 92°C for 30 min. The solution was then immediately placed in ice and kept at 4°C until use. These conditions led to the formation of aggregates with a hydrodynamic radius R_h of 70 nm, as measured by dynamic light scattering (Vasco Cordouan Technologies, $\lambda = 658$ nm).

Beforehand, pectin with 35% deesterified carboxyl groups (Cargill, Malchin, Allemagne) was purified to remove any traces of calcium chloride or magnesium ions. Pectins (5–10 g) were solubilized at 1% in distilled water. An ethylenediaminetetraacetic acid solution (EDTA, Sigma–Aldrich, CAS number 60-00-4, 0.5 mol L^{-1}, pH 8.0) was added once the pectin was solubilized to had 0.035 mol L^{-1} in the pectin solution. The pH of the pectin solution was adjusted to 8.0 with a 1 mol L^{-1} NaOH solution. It was then dialzsed, with a 14 000 Da retention threshold membrane, against distilled water for 10 days until a low and stable conductivity was reached. The solution was filtered through a cellulose nitrate filter with a pore size of 5 µm before freeze-drying. Finally, a 3% w/w solution of pectin was obtained by dissolving purified pectin in pure water.

The solution of alginate was prepared by dissolving alginate powder (CAS number 9005-38-3) in pure water to obtain a final solution of 3% alginate.

A 6 M stock solution of Ca^{2+} was prepared by dissolving calcium chloride powder ($CaCl_2$, $2H_2O$) (Sigma–Aldrich, CAS number 10035-04-8) in distilled water and diluted from 5.6 M to 21 mM.

Labeling Procedure: Proteins were covalently labeled by Rhodamine B isothiocyanate (RITC) according to the procedure used by [37–39]. RITC (CAS number 36877-69-7) as well as the solvent Dimethyl sulfoxide (DMSO, CAS number 67-68-5) are purchased from Sigma–Aldrich. RITC was dissolved at 2.4×10^{-3} M in DMSO. This stock solution was then mixed with a 15% protein solution to obtain final concentrations of RITC of 1 M and WPI $A = 15.7 \times 10^{-3}$ M. The pH was then adjusted to 9.5 before wrapping the bottle in aluminum foil and let to incubate for 10 h under slow agitation at room temperature. Then, the reaction was stopped with a solution of ethanolamine at 1.14×10^{-4} M (Sigma–Aldrich CAS number 141-43-5) and dialyzed to remove the unbound fluorescent dyes. Final WPI concentration was measured by UV absorption at 280 nm using an extinction coefficient of 1.0061 L g^{-1} cm^{-1}. Then the concentration of WPI and the pH were adjusted as described in the previous section before the thermal treatment to obtain fluorescent aggregates.

Experimental Set Up: Suspensions were gelled in a glass capillary of rectangular cross-section (1 × 0.1 mm) and 50 mm length, Figure 2A. The capillary was filled by capillarity, which results in two free interfaces, one at the end of the capillary being flat and which was put into contact with the calcium chloride solution, while the other end forms a meniscus inside the capillary, whose position is used to measure the flow rate. In the experiments where a pressure difference was imposed, the capillary was filled by connecting it to a reservoir containing the suspension of colloids. It was tested that the shell formation process is independent of the thickness of the capillary.

In both cases, the filled capillary was fixed on a glass slide and placed under a fluorescent microscope (Zeiss Axiovert 200M, lens ×4). A drop of calcium chloride was placed on the same glass slide. At $t = 0$ the capillary was carefully approached to the drop until they come into contact. The gelation front then propagated inside the capillary inducing a change in luminosity which allows to track its position over time. Gelation was observed by bright-field or wide-field fluorescence imaging and a black and withe camera Basler a2A1920-160umPRO.

Supporting Information

Supporting Information is available from the Wiley Online Library or from the author.

Acknowledgements

The authors are thankful to Ariane Gauge for performing some of the reaction front experiences. The authors thank also Laurent Heux and Maeva Touzard for insightful discussions and for providing the purified samples of pectin. LRP is part of the LabEx Tec21 (ANR-11-LABX-0030) and of the PolyNat Carnot Institute (ANR-11-CARN-007-01).

Conflict of Interest

The authors declare no conflict of interest.

Data Available Statement

The data that support the findings of this study are available from the corresponding author upon reasonable request.

Keywords

hydrogel, osmosis, permeation, structuration

Received: January 16, 2024
Revised: April 10, 2024
Published online:

[1] J. Idaszek, M. Costantini, T. A. Karlsen, J. Jaroszewicz, C. Colosi, S. Testa, E. Fornetti, S. Bernardini, M. Seta, K. Kasarełło, R. Wrzesien, S. Cannata, A. Barbetta, C. Gargioli, J. E. Brinchman, W. Swieszkowski, *Biofabrication* **2019**, *11*, 044101.
[2] M. Wang, W. Li, L. S. Mille, T. Ching, Z. Luo, G. Tang, C. E. Garciamendez, A. Lesha, M. Hashimoto, Y. S. Zhang, *Adv. Mater.* **2022**, *34*, 2107038.
[3] H. Jo, M. Yoon, M. Gajendiran, K. Kim, *Macromol. Biosci.* **2020**, *20*, 1900300.

[4] R. Levato, T. Jungst, R. G. Scheuring, T. Blunk, J. Groll, J. Malda, *Adv. Mater.* **2020**, *32*, 1906423.
[5] O. Erol, A. Pantula, W. Liu, D. H. Gracias, *Adv. Mater. Technol.* **2019**, *4*, 1900043.
[6] N. Zinkovska, J. Smilek, M. Pekar, *Polymers* **2020**, *12*, 966.
[7] J. Guo, Y. Yu, H. Wang, H. Zhang, X. Zhang, Y. Zhao, *Small* **2019**, *15*, 1805162.
[8] D. Z. Gunes, *Curr. Opin. Food Sci.* **2018**, *21*, 57.
[9] F. Sordo, E.-R. Janecek, Y. Qu, V. Michaud, F. Stellacci, J. Engmann, T. J. Wooster, F. Sorin, *Adv. Mater.* **2019**, *31*, 1807282.
[10] G. Bian, N. Pan, Z. Luan, X. Sui, W. Fan, Y. Xia, K. Sui, L. Jiang, *Angew. Chem.* **2021**, *133*, 20456.
[11] O. Lieleg, K. Ribbeck, *Trends Cell Biol.* **2011**, *21*, 543.
[12] M. K. Yazdi, V. Vatanpour, A. Taghizadeh, M. Taghizadeh, M. R. Ganjali, M. T. Munir, S. Habibzadeh, M. R. Saeb, M. Ghaedi, *Mater Sci Eng, C* **2020**, *114*, 111023.
[13] B. Gumuscu, A. S. Haase, A. M. Benneker, M. A. Hempenius, A. van den Berg, R. G. Lammertink, J. C. Eijkel, *Adv. Funct. Mater.* **2016**, *26*, 8685.
[14] W. Chen, Q. Wang, J. Chen, Q. Zhang, X. Zhao, Y. Qian, C. Zhu, L. Yang, Y. Zhao, X.-Y. Kong, B. Lu, L. Jiang, L. Wen, *Nano Lett.* **2020**, *20*, 5705.
[15] T. B. Schroeder, A. Guha, A. Lamoureux, G. VanRenterghem, D. Sept, M. Shtein, J. Yang, M. Mayer, *Nature* **2017**, *552*, 214.
[16] S. Marbach, L. Bocquet, *Chem. Soc. Rev.* **2019**, *48*, 3102.
[17] R. B. Schoch, J. Han, P. Renaud, *Rev. Mod. Phys.* **2008**, *80*, 839.
[18] W. Chen, Q. Zhang, Y. Qian, W. Xin, D. Hao, X. Zhao, C. Zhu, X.-Y. Kong, B. Lu, L. Jiang, L. Wen, *ACS Cent. Sci.* **2020**, *6*, 2097.
[19] P. Bacchin, J. Leng, J.-B. Salmon, *Chem. Rev.* **2021**, *122*, 6938.
[20] A. Staverman, *Recueil des Trav. Chim. des Pays-Bas* **1951**, *70*, 344.
[21] O. Kedem, A. Katchalsky, *Biochim. Biophys. Acta* **1958**, *27*, 229.
[22] S. Jeyarajah, J. C. Allen, *J. Agric. Food Chem.* **1994**, *42*, 80.
[23] A. Kharlamova, T. Nicolai, C. Chassenieux, *Food Hydrocolloids* **2018**, *79*, 145.
[24] M. H. Oztop, K. L. McCarthy, M. J. McCarthy, M. Rosenberg, *J. Food Sci.* **2012**, *77*, E68.
[25] A. Saxena, A. E. García, *J. Phys. Chem. B* **2015**, *119*, 219.
[26] M. Verheul, S. P. Roefs, *J. Agric. Food Chem.* **1998**, *46*, 4909.
[27] K. Potter, B. J. Balcom, T. A. Carpenter, L. D. Hall, *Carbohydr. Res.* **1994**, *257*, 117.
[28] E. Secchi, T. Roversi, S. Buzzaccaro, L. Piazza, R. Piazza, *Soft Matter* **2013**, *9*, 3931.
[29] I. Fraeye, I. Colle, E. Vandevenne, T. Duvetter, S. Van Buggenhout, P. Moldenaers, A. Van Loey, M. Hendrickx, *Innov. Food Sci. Emerg. Technol.* **2010**, *11*, 401.
[30] M. B. Albro, N. O. Chahine, M. Caligaris, V. I. Wei, M. Likhitpanichkul, K. W. Ng, C. T. Hung, G. A. Ateshian, *J. Biomech. Eng.* **2006**, *129*, 503.
[31] G. Skjåk-Bræk, H. Grasdalen, O. Smidsrød, *Carbohydr. Polym.* **1989**, *10*, 31.
[32] A. Maire du Poset, A. Lerbret, F. Boué, A. Zitolo, A. Assifaoui, F. Cousin, *Biomacromolecules* **2019**, *20*, 2864.
[33] B. Thu, O. Gåserød, D. Paus, A. Mikkelsen, G. Skjåk-Bræk, R. Toffanin, F. Vittur, R. Rizzo, *Biopolymers* **2000**, *53*, 60.
[34] Ý. A. Mørch, I. Donati, B. L. Strand, G. Skjak-Braek, *Biomacromolecules* **2006**, *7*, 1471.
[35] A. Mikkelsen, A. Elgsaeter, *Biopolymers* **1995**, *36*, 17.
[36] A. Vilotte, C. de Loubens, D. Z. Gunes, C. Schmitt, H. Bodiguel, *ACS Appl. Polym. Mater.* **2022**, *4*, 4075.
[37] E. Kolodziejczyk, V. Petkova, J.-J. Benattar, M. E. Leser, M. Michel, *Colloids Surf. A* **2006**, *279*, 159.
[38] M. Li, M. A. Auty, J. A. O'Mahony, A. L. Kelly, A. Brodkorb, *Food Hydrocolloids* **2016**, *61*, 504.
[39] C. Schmitt, C. Sanchez, A. Lamprecht, D. Renard, C.-M. Lehr, C. G. de Kruif, J. Hardy, *Colloids Surf B Biointerfaces* **2001**, *20*, 267.